


Communication

Nanostructural Characterisation and Optical Properties of Sputter-Deposited Thick Indium Tin Oxide (ITO) Coatings

Andrius Subacius ¹, Bill Baloukas ², Etienne Bousser ^{1,2}, Steve J. Hinder ³, Mark A. Baker ³, Claus Rebholz ^{1,4,*}  and Allan Matthews ^{1,*}

¹ Department of Materials, University of Manchester, Manchester M13 9PL, UK;

andrius.subacius@postgrad.manchester.ac.uk (A.S.); etienne-2.bousser@polymtl.ca (E.B.)

² Department of Engineering Physics, Polytechnique Montréal, Montreal, QC H3T 1J4, Canada; bill.baloukas@polymtl.ca

³ Department of Mechanical Engineering Sciences, University of Surrey, Guildford GU2 7XH, UK; s.hinder@surrey.ac.uk (S.J.H.); m.baker@surrey.ac.uk (M.A.B.)

⁴ Department of Mechanical and Manufacturing Engineering, University of Cyprus, 1678 Nicosia, Cyprus

* Correspondence: claus@ucy.ac.cy (C.R.); allan.matthews@manchester.ac.uk (A.M.)

Received: 23 October 2020; Accepted: 18 November 2020; Published: 21 November 2020



Abstract: Indium tin oxide (ITO) thin films, used in many optoelectronic applications, are typically grown to a thickness of a maximum of a few hundred nanometres. In this work, the composition, microstructure and optical/electrical properties of thick ITO coatings deposited by radio frequency magnetron sputtering from a ceramic ITO target in an Ar/O₂ gas mixture (total O₂ flow of 1%) on unheated glass substrates are reported for the first time. In contrast to the commonly observed (200) or (400) preferential orientations in ITO thin films, the approximately 3.3 μm thick coatings display a (622) preferential orientation. The ITO coatings exhibit a purely nanocrystalline structure and show good electrical and optical properties, such as an electrical resistivity of $1.3 \times 10^{-1} \Omega \cdot \text{cm}$, optical transmittance at 550 nm of ~60% and optical band gap of 2.9 eV. The initial results presented here are expected to provide useful information for future studies on the synthesis of high-quality thick ITO coatings.

Keywords: indium tin oxide; ITO; coatings; magnetron sputtering; thickness; structure; optical properties

1. Introduction

Indium tin oxide (ITO) is one of the most widely used materials as a transparent conducting oxide and ITO thin films are used in many applications, such as flat-panel displays, touch screen panels, light emitting diodes, solar cells and electrochromic devices (“smart windows”) [1,2]. Although several techniques have been applied for ITO deposition (for example, chemical vapour deposition [3,4], electron beam evaporation [5–7], sol-gel [8,9], spray pyrolysis [10] and pulsed-laser deposition [11]), direct current (DC) [12–18] and radio frequency (RF) [17–27] magnetron sputtering are the most attractive and used methods, since thin films with high quality can be produced on an industrial scale in well-established production facilities.

The properties of ITO films are dependent on various deposition parameters in magnetron sputtering, such as substrate temperature [16], target to substrate distance [27], power to the target [16–19], working gas pressure [16,19], oxygen flow/partial pressure during reactive deposition [14–19,25,26] and film thickness [13,14,16,23]. ITO films are often grown at elevated temperatures ($\geq 200 \text{ }^\circ\text{C}$) [12,15,16,18,25,26], or at lower temperatures followed by a post-deposition annealing step [27], to achieve better combined

optical and electrical performance. However, for several applications low processing temperatures are required, e.g., for low-cost and temperature-sensitive substrates, such as polymers [13,14], and for the deposition onto semiconductor thin films, where a change in properties may occur upon annealing [28]. Oxygen is regularly used as a reactive gas during sputtering from oxide targets [12,14–19,22,25,26] to deposit more stoichiometric films and, therefore, decrease the concentration of oxygen vacancies, achieving preferential orientation of specific crystallographic growth directions and adjusting the optical and electrical properties [29].

Sputtered ITO films are typically grown to a maximum thickness of several hundred nanometers [13,14,17,19,23,26], but some researchers have deposited films with thickness values of around 1 μm [12,16]. In a very new study, $\sim 2 \mu\text{m}$ thick sputtered ITO films were used as a medium for unconventional tailoring and manipulation of the light-matter interaction [30]. Most recently, up to 3 μm thick ITO coatings produced by CVD with high conductivity and transparency for the manufacture of functional protective coatings on mirrors with a reflecting layer were described [3], but sputtered films with this thickness have, to the best of our knowledge, yet to be reported. In general, vapour-deposited protective coatings with thickness values of around 2–5 μm are used in many applications (e.g., nanocomposite hard coatings for tribological applications synthesised by magnetron sputtering [31], arc-evaporation [32] or electron-beam evaporation [33]). Here, we investigate the nanostructure and optical properties of $\sim 3.3 \mu\text{m}$ thick ITO coatings synthesised onto unheated glass substrates by RF magnetron sputtering in an Ar/O₂ gas mixture.

2. Materials and Methods

ITO coatings were deposited onto 16 unheated soda-lime glass substrates (25 mm \times 25 mm), arranged in a 4 \times 4 array, by RF magnetron sputtering from a ceramic three-inch ITO target (In₂O₃:SnO₂—90:10 wt.%) in a commercial MiniLab 060 sputtering system (Moorfield, Knutsford, UK). A base pressure of 4.1×10^{-7} mbar (4.1×10^{-5} Pa) was reached prior to depositions, which were then carried out in an Ar/O₂ gas mixture with the ratio of oxygen flow to argon + oxygen flow [$P_{\text{O}_2} = (\text{O}_2/(\text{Ar} + \text{O}_2)) \times 100\%$] chosen as 1%. The total gas pressure and RF power density were kept constant throughout the deposition processes at 4.67×10^{-3} mbar (4.67×10^{-1} Pa) and 0.5 W/cm², respectively. The distance between the target and the substrates (rotated at a speed of 20 rpm) was set at 120 mm.

The crystalline structure was studied using a Bruker D8 Advance X-ray diffractometer (Middlesex, MA, USA) in grazing incidence angle mode at 3° and a 2 θ range between 15° and 70°. Copper K α radiation ($\lambda = 1.5405 \text{ \AA}$) was used for the measurements. X-ray photoelectron spectroscopy (XPS) spectra and depth profiles were recorded on a ThermoFisher Scientific Instruments (East Grinstead, UK) K-Alpha⁺ spectrometer using a monochromated Al K α X-ray source ($h\nu = 1486.6 \text{ eV}$) employing an X-ray spot of 400 μm radius (for surface spectra) and 200 μm radius (for depth profiles). High-energy resolution In 3d, Sn 3d and O 1s core level spectra were acquired using a pass energy of 50 eV and binding energies referenced to the adventitious C 1s peak at 285.0 eV. Quantification was performed utilising ThermoFisher Scientific Avantage software (Version: v5.9911), using a non-linear Shirley background and applying appropriate sensitivity factors, corrected for the electron energy analyser transmission function. XPS depth profiles were recorded using 3 keV Ar⁺ and a current of 2.3 μA . The rastered ion beam crater was set to a nominal size of 1 mm².

Surface roughness and atomic force microscopy (AFM) topological images of 2 μm \times 2 μm areas were acquired using a Bruker Multi Mode 8 atomic force microscope (Middlesex, MA, USA) in tapping mode. Scanning electron microscopy (SEM) images were acquired using a FEI Magellan scanning electron microscope (East Grinstead, UK) at an accelerating voltage of 10 keV. Optical transmission spectra for s- and p-polarized light at an angle of 6 degrees were measured with an Agilent Technologies Cary 7000 universal measurement spectrophotometer (UMS, Santa Clara, CA, USA). RGB colour coordinates were calculated for a standard CIE (Commission Internationale de l'Éclairage)

1931 2° observer and under illuminant CIE D65 (380 nm to 780 nm every 1 nm). The coatings' sheet resistance was measured with a four-point probe setup.

3. Results

3.1. Deposition

The rather large distance between the target and the rotating soda-lime glass substrates (120 mm, which is approximately twice the commonly used distance [14,16,18–20,24–26]), resulted in a deposition rate of only approximately 0.6 Å/s but allowed the temperature to remain below 40 °C during the approximately 15 h long deposition runs. All deposited ITO coatings (on the 16 glass slides/batch and between coating runs) showed a thickness deviation of less than 10%, as measured by SEM on coating cross-sections.

3.2. Structure and Phase Analysis

X-ray diffraction (XRD) diffractograms of an uncoated glass substrate and a thick ITO coating are presented in Figure 1. The ITO coating exhibits a purely nanocrystalline structure with an average grain size, determined from the (400) peak using the Scherrer equation, of approximately 24 nm and shows a (622) preferential orientation, which is rather unusual. The closest match found in the literature is from Kurdesau et al., who have reported crystalline 300 nm thick ITO films deposited by RF magnetron sputtering in an Ar–O₂ (3.0 vol.%) gas mixture at room temperature with strong (222), (400), (440) and (622) peaks and very similar minor XRD peaks as in the ITO coating reported here [17]. Das et al. have observed the decrease and finally absence of the (440) and (222) peaks for approximately 700 nm thick ITO films deposited by RF magnetron sputtering at 300 °C with an increase in the oxygen partial flow to 2.66%, where the films became more amorphous (an amorphous hump appearing in the XRD diffractograms between ~20°–40° (2θ)) and a (622) preferential orientation was detected [26]. Other researchers have also reported an increase in the (622) peak intensity upon incorporation of 0.5% O₂ in the Ar process gas in DC and RF magnetron sputtered ITO films grown at 300 °C [18] and with increasing O₂ flow in reactively DC magnetron-sputtered ITO thin films on unheated substrates [15]. However, in both of these studies the 300 nm thin films were still (222) or (400) preferentially oriented. Most recently, Bhorde et al. showed that with increasing RF power (and, therefore, deposition rate and thickness) for ITO films grown in Ar, showing mainly (222), (440) and (622) diffraction planes, the preferential crystal orientation changes from (222) to (400) [20].

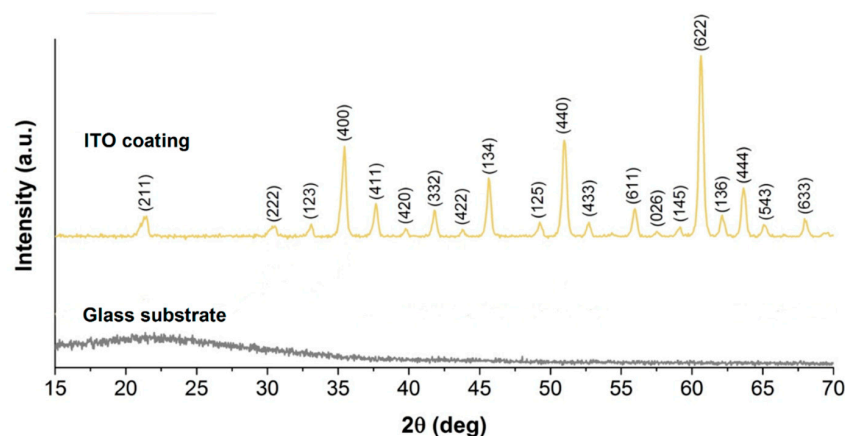


Figure 1. X-ray diffractograms of an uncoated glass substrate and a 3.3 μm thick ITO coating.

Others [11,16] have also found that the (400/222) peak intensity ratio increases with film thickness. Jung and Lee have considered not only process conditions, but also the physical and thermodynamic factors affecting the preferential orientation [16]. They concluded that a higher adatom mobility tends

to favour the growth of the thermodynamically favourable, lower surface energy (400) orientation, while a lower adatom mobility gives rise to the higher surface energy (222) orientation. Unfortunately, their XRD scans did not include higher angles, where the (622) peak occurs. For the ITO coatings deposited here, Figure 1 shows the (222) peak to be strongly suppressed, thus, there is clearly a preferred (400) orientation compared to (222) orientation for this coating, suggesting that there is a high surface mobility, in agreement with the observed purely crystalline structure.

3.3. Composition and Morphology

The XPS spectra of the coatings showed the following core level peak binding energies: In 3d_{5/2} at 444.3 ± 0.1 eV, Sn 3d_{5/2} at 486.6 ± 0.1 eV and O 1s at 529.9 ± 0.1 eV. These binding energies agree well with other work on ITO thin films [9,34]. A representative XPS depth profile given in Figure 2a shows the composition to be very consistent throughout the thickness. The coating is slightly sub-stoichiometric in oxygen. The average composition was determined to be 59.2 at.% O, 37.7 at.% In and 3.1 at.% Sn, giving a stoichiometry of In_{1.88}Sn_{0.16}O_{2.96}. These results are in very good agreement with Rutherford backscattering spectrometry (RBS) measurements recorded using a 3.3 MeV ⁴He⁺ primary beam, showing O concentrations of 58.5 at.%. It should be noted that the differences in O concentration between XPS and RBS are within experimental error. Although O₂ is commonly used as a reactive gas during sputtering from oxide targets to reduce the oxygen deficiency and form stoichiometric ITO films, in most reported work on sputtered ITO films only structural properties are presented. Das et al. reported very similar compositions for RF magnetron sputtered films deposited in Ar (59.3 at.% O) and with a ratio of O₂ to Ar + O₂ flow of 1.33% (62.9 at.% O) [26]. With regard to the presence of hydrogen from residual gases in ITO coatings (observed in preliminary atom probe tomography measurements to be at around 5 at.% in the coatings reported here), it has very recently been reported that the addition of small amounts of hydrogen (Ar + 5% H₂) in the working gas does not substantially change the crystallinity of ITO films but decreases the resistivity [21], since the presence of hydrogen is expected to remove oxygen from the ITO films and, therefore, promotes the formation of oxygen vacancies [29,35].

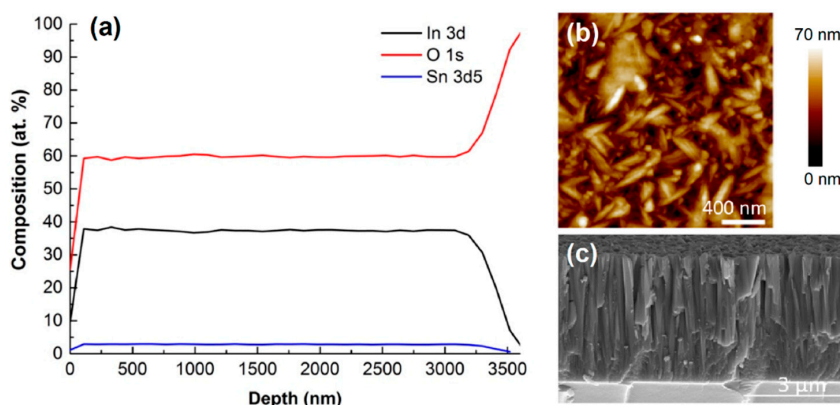


Figure 2. (a) XPS depth profile, showing the elemental composition as a function of depth, (b) an AFM topographical image with an Rq value of 10.5 nm and (c) the SEM cross-section image of the same 3.3 μm thick ITO coating.

The AFM and SEM images in Figure 2b,c are consistent with the XRD data. The displayed ITO coating exhibits a faceted surface structure in the AFM image (Figure 2b), which would be expected from a nanocrystalline structure, and a columnar microstructure in the SEM cross-section (Figure 2c). Gorjanc et al. reported similar columnar structures for thinner ITO films deposited by RF magnetron sputtering at room temperature when adding very small O₂ flows (0.21–0.63 sccm) to 100 sccm Ar [19], and Najwa et al. observed a nanocolumnar structure for ~500 nm thick films deposited by RF magnetron sputtering at 200 °C at an Ar/O₂ ratio of 14:1 (7% O₂) [22]. Unfortunately, in both studies no compositional data are included.

3.4. Optical Properties

One critical parameter of ITO coatings is their optical transparency. The photograph in Figure 3 shows a yellow (RGB = 226,205,101) colour for the ITO coating. As stated earlier, the oxygen content in ITO films is a critical parameter affecting both their transparency and conductivity. Higher oxygen concentrations result in fewer oxygen vacancies and highly resistive films. In this work, the resistivity of the coatings increased with the introduction of 1% O₂ during coating deposition to $1.3 \times 10^{-1} \Omega\cdot\text{cm}$ (from $5.29 \times 10^{-4} \Omega\cdot\text{cm}$ for coatings deposited in pure Ar; not shown here). Similar values have been reported for sputter-deposited ITO coatings in Ar and Ar/O₂ gas mixtures [19,25]. Figure 3 shows the transmittance of a thick ITO coating between 300 nm and 2500 nm, where an uncoated glass substrate is shown for comparison. The transmittance curve of the ITO coating shows ~60% at 550 nm. Transmittance values in ITO films are known to decrease with increasing thickness [12–14,23,24], mainly due to absorption. For example, Kim et al. reported a drop in transmittance at 550 nm from ~85% to ~75% with an increase in the thickness from 100 to 1000 nm for ITO films deposited in an Ar/O₂ mixture [12]. An optical bandgap of 2.9 eV was calculated using Tauc's relation. This value is lower than the typically ~3.4–3.9 eV reported for ITO [27]. Oxygen-deficient films, such as those reported here, have narrower bandgaps, resulting in a redshift of the optical transmittance spectrum [19].

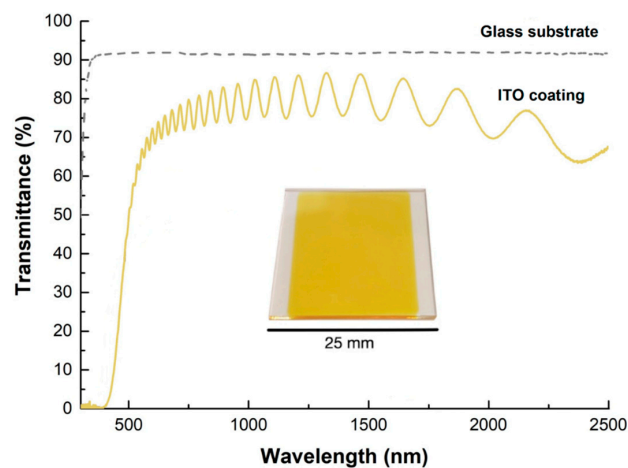


Figure 3. Optical transmission spectra of an uncoated glass substrate and a 3.5 μm thick ITO coating. A photograph of the coated glass slide is shown in the middle.

4. Conclusions

The structure and optical properties of ~3.3 μm thick ITO coatings deposited by radio frequency magnetron sputtering from a ceramic ITO target in an Ar/O₂ gas mixture (total O₂ flow of 1%) on unheated glass substrates was investigated. The coatings exhibit a (622) preferential orientation and a nanocrystalline structure and display good electrical resistivity, optical transmittance at 550 nm and optical band gap values of $1.3 \times 10^{-1} \Omega\cdot\text{cm}$, ~60% and 2.9 eV, respectively.

This study has shown that micrometre thick ITO coatings with good performance can be synthesised by sputter deposition at low temperature. These initial results are expected to provide useful information and will help to guide future studies on the synthesis of high quality ITO coatings. For example, as protective coatings for facets in mirror-concentration systems to increase the service life of such mirrors under open atmospheric conditions and as thick epsilon-near-zero ITO metafilms for applications in optical communications, RF-photonics and integrated silicon photonics. The composition, structure and properties of such coatings can be tuned by adjusting the Ar/O₂ gas mixture flow during deposition and/or by additional post-deposition treatments.

Author Contributions: Conceptualization: A.S., C.R., and A.M.; methodology: C.R., B.B., and E.B.; software: A.S.; validation: E.B. and M.A.B.; investigation: A.S., B.B., E.B., and S.J.H.; resources: A.M.; data curation:

S.A.; writing—original draft preparation: A.S. and C.R.; writing—review and editing: E.B., M.A.B., and A.M.; visualization: A.S. and C.R.; supervision: C.R. and A.M.; project administration: A.M.; funding acquisition: A.M. All authors have read and agreed to the published version of the manuscript.

Funding: This research was funded by the European Research Council under the ERC Advanced Grant ‘IMPUNEP’, grant number 320879. The APC was funded by the University of Cyprus.

Acknowledgments: The authors are grateful to Pierre Couture and Jonathan England (UK National Ion Beam Centre, University of Surrey) for providing RBS measurements.

Conflicts of Interest: The authors declare no conflict of interest.

References

1. Ellmer, K. Past achievements and future challenges in the development of optically transparent electrodes. *Nat. Photonics* **2012**, *6*, 809–817. [[CrossRef](#)]
2. Granqvist, C.G. Transparent conductors as solar energy materials: A panoramic review. *Sol. Energy Mater. Sol. Cells* **2007**, *91*, 1529–1598. [[CrossRef](#)]
3. Atabaev, I.G.; Khazhiev, M.U.; Zakirova, S.B.; Shermatov, Z. Correlation between the structure, specific resistance, and optical properties of ITO films grown by CVD. *Appl. Sol. Energy (Engl. Transl. Geliotekhnika)* **2017**, *53*, 322–325. [[CrossRef](#)]
4. Maki, K.; Komiya, N.; Suzuki, A. Fabrication of thin films of ITO by aerosol CVD. *Thin Solid Films* **2003**, *445*, 224–228. [[CrossRef](#)]
5. Senthilkumar, V.; Vickraman, P.; Jayachandran, M.; Sanjeeviraja, C. Structural and optical properties of indium tin oxide (ITO) thin films with different compositions prepared by electron beam evaporation. *Vacuum* **2010**, *84*, 864–869. [[CrossRef](#)]
6. El-Nahass, M.M.; El-Menyawy, E.M. Thickness dependence of structural and optical properties of indium tin oxide nanofiber thin films prepared by electron beam evaporation onto quartz substrates. *Mater. Sci. Eng. B Solid-State Mater. Adv. Technol.* **2012**, *177*, 145–150. [[CrossRef](#)]
7. Nuchuay, P.; Chaikereee, T.; Horprathum, M.; Mungkung, N.; Kasayapanand, N.; Oros, C.; Limwichean, S.; Nuntawong, N.; Chananonwathorn, C.; Patthanasettakul, V.; et al. Engineered omnidirectional antireflection ITO nanorod films with super hydrophobic surface via glancing-angle ion-assisted electron-beam evaporation deposition. *Curr. Appl. Phys.* **2017**, *17*, 222–229. [[CrossRef](#)]
8. Biswas, N.; Ghosh, P.; Sarkar, S.; Moitra, D.; Biswas, P.K.; Jana, S.; Mukhopadhyay, A.K. Nanomechanical properties of dip coated indium tin oxide films on glass. *Thin Solid Films* **2015**, *579*, 21–29. [[CrossRef](#)]
9. An, J.S.; Kim, S.C.; Hahn, S.H.; Ko, S.K.; Kim, E.J. Influence of annealing on the optical and the electrical properties of ITO thin films prepared by using a sol-gel spin method. *J. Korean Phys. Soc.* **2004**, *45*, 1629–1634.
10. Zhang, L.; Lan, J.; Yang, J.; Guo, S.; Peng, J.; Zhang, L.; Tian, S.; Ju, S.; Xie, W. Study on the physical properties of indium tin oxide thin films deposited by microwave-assisted spray pyrolysis. *J. Alloys Compd.* **2017**, *728*, 1338–1345. [[CrossRef](#)]
11. Kim, H.; Horwitz, J.S.; Kushto, G.; Piqué, A.; Kafafi, Z.H.; Gilmore, C.M.; Chrisey, D.B. Effect of film thickness on the properties of indium tin oxide thin films. *J. Appl. Phys.* **2000**, *88*, 6021–6025. [[CrossRef](#)]
12. Kim, J.H.; Seong, T.Y.; Ahn, K.J.; Chung, K.B.; Seok, H.J.; Seo, H.J.; Kim, H.K. The effects of film thickness on the electrical, optical, and structural properties of cylindrical, rotating, magnetron-sputtered ITO films. *Appl. Surf. Sci.* **2018**, *440*, 1211–1218. [[CrossRef](#)]
13. Eshaghi, A.; Graeli, A. Optical and electrical properties of indium tin oxide (ITO) nanostructured thin films deposited on polycarbonate substrates “thickness effect”. *Optik* **2014**, *125*, 1478–1481. [[CrossRef](#)]
14. Hao, L.; Diao, X.; Xu, H.; Gu, B.; Wang, T. Thickness dependence of structural, electrical and optical properties of indium tin oxide (ITO) films deposited on PET substrates. *Appl. Surf. Sci.* **2008**, *254*, 3504–3508. [[CrossRef](#)]
15. Sittinger, V.; Ruske, F.; Werner, W.; Jacobs, C.; Szyzka, B.; Christie, D.J. High power pulsed magnetron sputtering of transparent conducting oxides. *Thin Solid Films* **2008**, *516*, 5847–5859. [[CrossRef](#)]
16. Jung, Y.S.; Lee, S.S. Development of indium tin oxide film texture during DC magnetron sputtering deposition. *J. Cryst. Growth* **2003**, *259*, 343–351. [[CrossRef](#)]
17. Kurdesau, F.; Khripunov, G.; da Cunha, A.F.; Kaelin, M.; Tiwari, A.N. Comparative study of ITO layers deposited by DC and RF magnetron sputtering at room temperature. *J. Non-Cryst. Solids* **2006**, *352*, 1466–1470. [[CrossRef](#)]

18. Qiao, Z.; Mergel, D. Comparison of radio-frequency and direct-current magnetron sputtered thin In_2O_3 : Sn films. *Thin Solid Films* **2005**, *484*, 146–153. [[CrossRef](#)]
19. Gorjanc, T.C.; Leong, D.; Py, C.; Roth, D. Room temperature deposition of ITO using r.f. magnetron sputtering. *Thin Solid Films* **2002**, *413*, 181–185. [[CrossRef](#)]
20. Bhorde, A.; Jadhavar, A.; Waykar, R.; Nair, S.; Borate, H.; Pandharkar, S.; Aher, R.; Naik, D.; Vairale, P.; Lonkar, G.; et al. (400)-Oriented indium tin oxide thin films with high mobility and figure of merit prepared by radio frequency magnetron sputtering. *Thin Solid Films* **2020**, *704*, 137972. [[CrossRef](#)]
21. Sousa, M.G.; da Cunha, A.F. Optimization of low temperature RF-magnetron sputtering of indium tin oxide films for solar cell applications. *Appl. Surf. Sci.* **2019**, *484*, 257–264. [[CrossRef](#)]
22. Najwa, S.; Shuhaimi, A.; Talik, N.A.; Ameer, N.; Sobri, M.; Rusop, M. In-situ tuning of Sn doped In_2O_3 (ITO) films properties by controlling deposition Argon/Oxygen flow. *Appl. Surf. Sci.* **2019**, *479*, 1220–1225. [[CrossRef](#)]
23. Amalathas, A.P.; Alkai, M.M. Effects of film thickness and sputtering power on properties of ITO thin films deposited by RF magnetron sputtering without oxygen. *J. Mater. Sci. Mater. Electron.* **2016**, *27*, 11064–11071. [[CrossRef](#)]
24. Ghorannevis, Z.; Akbarnejad, E.; Ghorannevis, M. Structural and morphological properties of ITO thin films grown by magnetron sputtering. *J. Theor. Appl. Phys.* **2015**, *9*, 285–290. [[CrossRef](#)]
25. Kim, J.H.; Lee, J.H.; Heo, Y.W.; Kim, J.J.; Park, J.O. Effects of oxygen partial pressure on the preferential orientation and surface morphology of ITO films grown by RF magnetron sputtering. *J. Electroceramics* **2009**, *23*, 169–174. [[CrossRef](#)]
26. Das, R.; Adhikary, K.; Ray, S. The role of oxygen and hydrogen partial pressures on structural and optical properties of ITO films deposited by reactive rf-magnetron sputtering. *Appl. Surf. Sci.* **2007**, *253*, 6068–6073. [[CrossRef](#)]
27. Antony, A.; Nisha, M.; Manoj, R.; Jayaraj, M.K. Influence of target to substrate spacing on the properties of ITO thin films. *Appl. Surf. Sci.* **2004**, *225*, 294–301. [[CrossRef](#)]
28. Hotovy, J.; Hüpkens, J.; Böttler, W.; Marins, E.; Spiess, L.; Kups, T.; Smirnov, V.; Hotovy, I.; Kováč, J. Sputtered ITO for application in thin-film silicon solar cells: Relationship between structural and electrical properties. *Appl. Surf. Sci.* **2013**, *269*, 81–87. [[CrossRef](#)]
29. Lee, Y.-L.; Lee, K.-M. Effect of ambient gases on the characteristics of ITO thin films for OLEDs. *Trans. Electr. Electron. Mater.* **2009**, *10*, 203–207. [[CrossRef](#)]
30. Ni, J.H.; Sarney, W.L.; Leff, A.C.; Cahill, J.P.; Zhou, W. Property variation in wavelength-thick epsilon-near-zero ITO metafilm for near IR photonic devices. *Sci. Rep.* **2020**. [[CrossRef](#)]
31. Polychronopoulou, K.; Rebholz, C.; Baker, M.A.; Theodorou, L.; Demas, N.G.; Hinder, S.J.; Polycarpou, A.A.; Dumanidis, C.C.; Böbel, K. Nanostructure, mechanical and tribological properties of reactive magnetron sputtered TiC_x coatings. *Diam. Relat. Mater.* **2008**, *17*, 2054–2061. [[CrossRef](#)]
32. Polychronopoulou, K.; Baker, M.A.; Rebholz, C.; Neidhardt, J.; O’Sullivan, M.; Reiter, A.E.; Kanakis, K.; Leyland, A.; Matthews, A.; Mitterer, C. The nanostructure, wear and corrosion performance of arc-evaporated CrB_xN_y nanocomposite coatings. *Surf. Coat. Technol.* **2009**, *204*, 246–255. [[CrossRef](#)]
33. Rebholz, C.; Monclus, M.A.; Baker, M.A.; Mayrhofer, P.H.; Gibson, P.N.; Leyland, A.; Matthews, A. Hard and superhard TiAlBN coatings deposited by twin electron-beam evaporation. *Surf. Coat. Technol.* **2007**, *201*. [[CrossRef](#)]
34. Gassenbauer, Y.; Schafranek, R.; Klein, A.; Zafeiratos, S.; Hävecker, M.; Knop-Gericke, A.; Schlögl, R. Surface states, surface potentials, and segregation at surfaces of tin-doped In_2O_3 . *Phys. Rev. B Condens. Matter Mater. Phys.* **2006**, *73*, 1–11. [[CrossRef](#)]
35. Luo, S.; Kohiki, S.; Okada, K.; Shoji, F.; Shishido, T. Hydrogen effects on crystallinity, photoluminescence, and magnetization of indium tin oxide thin films sputter-deposited on glass substrate without heat treatment. *Phys. Status Solidi Appl. Mater. Sci.* **2010**, *207*, 386–390. [[CrossRef](#)]

Publisher’s Note: MDPI stays neutral with regard to jurisdictional claims in published maps and institutional affiliations.



© 2020 by the authors. Licensee MDPI, Basel, Switzerland. This article is an open access article distributed under the terms and conditions of the Creative Commons Attribution (CC BY) license (<http://creativecommons.org/licenses/by/4.0/>).